STEM CELLS TRANSLATIONAL MEDICINE®

CELL-BASED DRUG DEVELOPMENT, SCREENING, AND TOXICOLOGY

Induced Pluripotent Stem Cells for Disease Modeling and Evaluation of Therapeutics for Niemann-Pick Disease Type A

YAN LONG,[a,b] MIAO XU,[a,c] RONG LI,[a] SHENG DAI,[a,c] JEANETTE BEERS,[d] GUOKAI CHEN,[d,e] FERRI SOHEILIAN,[f] ULRICH BAXA,[f] MENGQIAO WANG,[a] JUAN J. MARUGAN,[a] SILVIA MURO,[g,h] ZHIYUAN LI,[b] ROSCOE BRADY,[i] WEI ZHENG[a]

[a]National Center for Advancing Translational Sciences, [d]Center for Molecular Medicine, National Heart, Lung, and Blood Institute, and [i]National Institute of Neurological Disorders and Stroke, National Institutes of Health, Bethesda, Maryland, USA; [b]Guangzhou Institutes of Biomedicine and Health, Chinese Academy of Sciences, Guangzhou, People's Republic of China; [c]Sir Run Run Shaw Hospital, Zhejiang University School of Medicine, Hangzhou, People's Republic of China; [e]Faculty of Health Sciences, University of Macau, Macau, People's Republic of China; [f]Electron Microscopy Laboratory, Cancer Research Technology Program, Leidos Biomedical Research, Inc., Frederick National Laboratory for Cancer Research, Frederick, Maryland, USA; [g]Institute for Bioscience and Biotechnology Research and [h]Fischell Department of Bioengineering, University of Maryland, College Park, Maryland, USA

Correspondence: Wei Zheng, Ph.D., National Center for Advancing Translational Sciences, National Institutes of Health, 9800 Medical Center Drive, MSC 3375, Bethesda, Maryland 20892, USA. Telephone: 301-217-5251; E-Mail: wzheng@mail.nih.gov

Received December 3, 2015; accepted for publication May 13, 2016; published Online First on August 2, 2016.

1066-5099/2016/$20.00/0

http://dx.doi.org/10.5966/sctm.2015-0373

Key Words. Niemann-Pick disease type A • Induced pluripotent stem cells • Differentiated neural stem cells • Cyclodextrin • δ-Tocopherol • α-Tocopherol • Acid sphingomyelinase

ABSTRACT

Niemann-Pick disease type A (NPA) is a lysosomal storage disease caused by mutations in the *SMPD1* gene that encodes acid sphingomyelinase (ASM). Deficiency in ASM function results in lysosomal accumulation of sphingomyelin and neurodegeneration. Currently, there is no effective treatment for NPA. To accelerate drug discovery for treatment of NPA, we generated induced pluripotent stem cells from two patient dermal fibroblast lines and differentiated them into neural stem cells. The NPA neural stem cells exhibit a disease phenotype of lysosomal sphingomyelin accumulation and enlarged lysosomes. By using this disease model, we also evaluated three compounds that reportedly reduced lysosomal lipid accumulation in Niemann-Pick disease type C as well as enzyme replacement therapy with ASM. We found that α-tocopherol, δ-tocopherol, hydroxypropyl-β-cyclodextrin, and ASM reduced sphingomyelin accumulation and enlarged lysosomes in NPA neural stem cells. Therefore, the NPA neural stem cells possess the characteristic NPA disease phenotype that can be ameliorated by tocopherols, cyclodextrin, and ASM. Our results demonstrate the efficacies of cyclodextrin and tocopherols in the NPA cell-based model. Our data also indicate that the NPA neural stem cells can be used as a new cell-based disease model for further study of disease pathophysiology and for high-throughput screening to identify new lead compounds for drug development. STEM CELLS TRANSLATIONAL MEDICINE *2016;5:1644–1655*

SIGNIFICANCE

Currently, there is no effective treatment for Niemann-Pick disease type A (NPA). To accelerate drug discovery for treatment of NPA, NPA-induced pluripotent stem cells were generated from patient dermal fibroblasts and differentiated into neural stem cells. By using the differentiated NPA neuronal cells as a cell-based disease model system, α-tocopherol, δ-tocopherol, and hydroxypropyl-β-cyclodextrin significantly reduced sphingomyelin accumulation in these NPA neuronal cells. Therefore, this cell-based NPA model can be used for further study of disease pathophysiology and for high-throughput screening of compound libraries to identify lead compounds for drug development.

INTRODUCTION

Niemann-Pick disease type A (NPA) is a rare autosomal recessive disorder with an incidence of 0.5 to 1 per 100,000 births [1]. NPA is caused by mutations in the *SMPD1* gene encoding for acid sphingomyelinase (ASM) [2], resulting in accumulation of sphingomyelin (SM) in lysosomes of patient cells [3]. The carrier frequency of NPA disease in the Ashkenazi Jewish population is approximately 1 in 90, with common mutations of fsP330, L302P, and R496L that account for approximately 97% of the mutations [4]. The clinical presentations of NPA include hepatosplenomegaly, psychomotor regression and neurologic deterioration, widespread lung damage, and an eye abnormality called a cherry-red spot [5, 6]. The affected children have a poor prognosis and usually die before age 3 years [7, 8].

Currently, there is no treatment for NPA. Enzyme replacement therapy (ERT) is available to treat several lysosomal storage diseases, including Gaucher disease; Fabry disease; Pompe disease; and mucopolysaccharidosis (MPS) types I, II, and VI [9, 10]. Intravenous infusion of the human recombinant enzyme to ASM knockout mice significantly reduced lipid storage only in the reticuloendothelial system [11]. It had no effect on the progression of neurological disease and

did not extend the survival time. ERT is not obviously suitable in NPA because the enzymes do not efficiently cross the blood-brain barrier [12]. Gene replacement by intracranial injection of viral vectors expressing human ASM was tested in ASM knockout mice; this approach alleviated storage abnormality in the brain and motor deficits [13]. However, application of gene therapy in human has still a long way to go because of the challenge of pre-existing immunity to the viral capsid proteins and safety concerns [14]. Delivery carriers to improve brain accumulation of recombinant enzymes have emerged [15], but these strategies are still under early development. Other therapeutic approaches are ineffective or unavailable, including hematopoietic stem cell transplantation [16], substrate reduction therapy [17], and pharmaceutical chaperone therapy [18].

It has been reported that δ-tocopherol reduced the lysosomal cholesterol accumulation in Niemann-Pick disease type C (NPC) patient cells through a mechanism of increased lysosomal exocytosis [19]. It also reduced the enlarged lysosome size in NPA patient fibroblasts [19]. Cyclodextrin had also been reported to reduce lysosomal cholesterol accumulation with more potent effect in patient neural stem cells differentiated from induced pluripotent stem cells (iPSCs) than that in patient fibroblasts [20]. A recent study has also showed that cyclodextrin reduced lipid storage in NPA fibroblasts [21]. The effects of tocopherols and cyclodextrin have not been evaluated on NPA neuronal cells. We report here the generation of four iPSC lines from two NPA patient fibroblasts with mutations of fsP330 and L302P. These NPA iPSCs were differentiated into neural stem cells that exhibited sphingomyelin accumulation. Using this NPA cell-based model, we evaluated the pharmacological effects of α-tocopherol, δ-tocopherol, cyclodextrin, and acid sphingomyelinase on reduction of lysosomal sphingomyelin accumulation. Our results demonstrate that the neural stem cells differentiated from NPA iPSCs is a useful disease model for further study of disease pathophysiology and for drug screening to identify new lead compounds for drug development.

Materials and Methods

Materials

BODIPY-FL C12−sphingomyelin (catalog no. D7711), Hoechst 33342 (H3570), CELLstart substrate (A1014201), and LysoTracker red (L7528) were obtained from Thermo Fisher Scientific Life Sciences (Waltham, MA, http://www.thermofisher.com). α-Tocopherol and δ-tocopherol were purchased from Sigma-Aldrich (St. Louis, MO, http://www.sigmaaldrich.com) and purified by high-performance liquid chromatography to a purity greater than 99%. We purchased 96-well plates from Greiner Bio-One (Monroe, NC, http://www.greinerbioone.com). Matrigel (354277) was obtained from Corning (San Jose, CA, https://www.corning.com), and Rock inhibitor Y-27632 was purchased from Tocris Bioscience (Ellisville, MO, https://www.tocris.com/). ASM was obtained from Sigma-Aldrich (S-5383). A human neural stem cell line (N7800100, H9-derived) was obtained from Thermo Fisher. Human skin fibroblast cell lines were purchased from the Coriell Cell Repository (Camden, NJ, https://catalog.coriell.org/), including wide-type cell line (GM05659) and lines from one female NPA patient (GM13205) and one male NPA patient (GM16195).

Generation of iPSCs

Primary skin fibroblasts from unaffected individuals (GM05659) and NPA patients carrying mutations in the *SMPD1* gene (GM13205 with deletion of a cytosine in codon 330 and GM16195 with T-C transition in the nucleotide 905) were cultured in Dulbecco's modified Eagle's medium (DMEM) with 10% fetal bovine serum/nonessential amino acids/GlutaMAX (Thermo Fisher) (supplemental online Table 1). The cells were reprogrammed by using the nonintegrating CytoTune-Sendai viral vector kit (Thermo Fisher) by following the method described previously [22]. Briefly, fibroblasts were plated at a high density in a 48-well plate, and the CytoTune-iPS 2.0 Sendai reprogramming kit was used to infect cells according to instructions. At day 4, cells were replated onto a Matrigel-coated dish in E8 media-based reprogramming media 2 and were fed every other day until day 20, when individual colonies were passaged by the EDTA dissociation method into separate wells in E8 medium. The selected iPSC colonies (2 for each patient sample) were further cultured beyond 15 passages.

Fluorescence-Activated Cell Sorting Analysis and Karyotyping of iPSCs

The iPSCs were harvested from 6-well plates using TrypLE Express enzyme (12605010, Thermo Fisher). Cells were fixed with 4% paraformaldehyde for 10 minutes at room temperature and then washed with PBS. Before fluorescence-activated cell sorting analysis, cells were permeabilized with 0.2% Tween-20 in phosphate-buffered saline (PBS) for 10 minutes at room temperature and stained with anti-Tra-1-60-fluorescein isothiocyanate (FITC) (FCMAB115F, EMD Millipore, Billerica, MA, http://www.emdmillipore.com/) and anti-Nanog-Alexa Fluor 488 (FCABS352A4, EMD Millipore) with the concentration recommended in the instruction. Nonimmune controls were used at 0.5 μl per 50-μl reaction, mouse-IgG2b-FITC (MABC006F, EMD Millipore), and rabbit IgG isotype-AlexaFluor 488 conjugate (4340S, Cell Signaling Technologies, Danvers, MA, https://www.cellsignal.com/). Cells were then analyzed on a BD Accuri C6 Flow Cytometry system (BD Biosciences, San Jose, CA, http://www.bdbiosciences.com).

The iPSCs were seeded in a T-25 flask, and the G-banding karyotype analysis was conducted at WiCell Research Institute (Madison, WI, https://www.wicell.org/). Cell harvest, slide preparation, and G-banded karyotyping were performed by using standard cytogenetic protocols. Cells were incubated with ethidium bromide and colcemid and then placed in hypotonic solution followed by fixation. Metaphase cell preparations were stained with Leishman stain. Twenty randomly selected metaphases were analyzed by G-banding for each cell line.

Induction of Neural Stem Cells From Human iPSCs and Immunofluorescence Staining of Neural Stem Cell Protein Markers

NPA iPSCs were differentiated to neural stem cells (NSCs) using the PSC Neural Induction Medium (A1647801, Life Technologies) following the protocol from the manufacture. Briefly, the iPSCs were cultured in feeder-free condition in Essential 8 Medium (A1517001, Thermo Fisher) on Matrigel human embryonic stem cell-qualified matrix (354277, Corning). When the iPSCs reach 70%–80% confluence, pluripotent stem cells are dislodged (PSC) with 0.5 mM EDTA buffer and then reseeded onto Matrigel-precoated 6-well plate at 3×10^5 cells/well in the E8 medium in the presence of 10 μM Rock inhibitor Y-27632 (1254, Tocris Bioscience). After cell attachment, cell culture medium was changed with the complete PSC neural induction medium containing neurobasal medium and 1$\times$ neural induction supplement (Thermo Fisher). The cells were cultured for another 7 days, and the cell culture medium was changed every

other day. At day 7 of neural induction, the initial NSCs were dissociated with the StemPro cell dissociation reagent (A11105, Thermo Fisher) and plated in the Matrigel-precoated T75 flasks for further expansion in the neural expansion medium containing neurobasal medium and Advanced DMEM/F12 (A12634, Thermo Fisher) at a 1:1 ratio, and 1× neural induction supplement.

NSCs were fixed in 4% paraformaldehyde for 15 minutes, rinsed with PBS, and permeabilized with 0.3% Triton X-100 for 15 minutes, followed by incubation with four primary antibodies: Oct4 (1:100 dilution, A13998, Thermo Fisher), Sox1 (1:100, AF3369, R&D Systems, Minneapolis, MN, https://www.rndsystems.com/), Sox2 (1:100, MAB2018, R&D Systems), and Nestin (1:1,000 dilution, 611658, BD Bioscience) overnight at 4°C. After washing with PBS, a corresponding secondary antibody conjugated with Alexa Fluor 647 (1:250 dilution, Thermo Fisher) was added. Cells were then stained with Hoechst 33342 for 20 minutes after a wash and were imaged using an IN Cell 2000 imaging system (GE Healthcare, Port Washington, NY, http://www.gehealthcare.com) with a ×20 objective lens and Cy5 and 4′,6-diamidino-2-phenylindole (DAPI) filter sets.

BODIPY-FL C12-Sphingomyelin Staining and LysoTracker Red Dye Staining

Cells were seeded into 96-well plates precoated with CELLstart (1:100 dilution in PBS). After 4-hour incubation at 37°C with 5% CO_2, 0.2 μg/ml BODIPY-FL C12−sphingomyelin (D7711) was added to cells and incubated for 24 hours [23]. The cells were then fixed in 100 μl/well 3.2% paraformaldehyde solution containing 1 μg/ml Hoechst 33342 (H3570) for 30 minute at room temperature in the dark, followed by three washes at room temperature with PBS. The fluorescence images were taken with the IN Cell 2000 imaging system using DAPI and FITC filter sets.

LysoTracker dye stains cellular acidic compartments that can be used to visualize enlarged lysosomes in patient cells at the proper dye concentration [19]. Briefly, 1,500 cells/well were seeded in black, clear-bottom, 96-well plates and treated with compounds for 4 days. The cells were washed with PBS and incubated with 50 nM LysoTracker red dye at 100 μl/well (L-7528) at 37°C for 1 hour. Next, the cells were fixed in 3.2% paraformaldehyde solution (100 μl/well) containing 1 μg/ml Hoechst 33342 (H3570) in PBS with an incubation at room temperature for 30 minutes. After cell washing, the cells were imaged in the INCell 2000 imaging system using DAPI and DsRed filter sets.

Images were analyzed with the multitarget analysis protocol (IN Cell imaging analysis software, GE Healthcare). Nuclei were segmented by using the top-hat segmentation method with a minimum area set at 75 μm and a sensitivity set at 50. Stained lysosomes were identified as "organelles" and were segmented by using the multiscale top-hat algorithm. Settings for lysosome detection included identification of granules ranging in size from 0.5 to 45 μm (3–13 pixels) and a sensitivity setting of 60. Total organelle intensity was calculated by a user-defined threshold for organelle intensity.

Electron Microscopy

Cells were fixed in 2% glutaraldehyde, 0.1 M sodium cacodylate, for 1 hour at room temperature (RT) and transferred to 4°C. All wells were washed three times with 0.1 M sodium cacodylate buffer, postfixed with 1% osmium tetroxide at RT for 1 hour, washed three times with 0.1 M sodium cacodylate buffer and once with 0.1M sodium acetate buffer, stained with 0.5% uranyl acetate (UA) for 1 hour, and washed twice again with 0.1 M sodium acetate buffer. The wells were dehydrated through a series of graded ethanol twice each (35%, 50%, 70%, and 95%) and three times with 100%. All wells were infiltrated with 100% epoxy resin overnight and then washed with 100% resin for 10 minutes each time. Resin was polymerized for 72 hours at 55°C. The cells of interest were cut, trimmed with razor blade, and thin sectioned (70–90 nm) with a diamond knife using a Leica EM UC6 ultramicrotome (Leica Microsystems, Buffalo Grove, IL, http://www.leica-microsystems.com). Sections were stained (1:1 0.25% UA and 35% ethyl alcohol for 2 minutes and 1:1 5% lead citrate and H_2O for 2 minutes), thinly carbon-coated in an Edwards carbon evaporator, and imaged using a Hitachi 7600 transmission electron microscope. Images were taken with an advanced microscopy techniques charge-coupled device camera.

Statistical Analysis

Concentration-response curves were analyzed and half maximal inhibitory concentration values were calculated by using Prism software (GraphPad, La Jolla, CA, http://www.graphpad.com/). The bottom value in the four-parameter fit was fixed at the minimal number because the concentration-response curves of compounds showed an incomplete inhibition at the bottom plateau due to the highest concentration used. Results in the figures are expressed as mean of triplicates ± SEM. Unless otherwise stated, unpaired *t* tests were used to test for significance; in the figures, * indicates $p < .05$ and ** **indicates** $p < .01$.

RESULTS

Generation of iPSC Lines From NPA Patient Fibroblasts and NSC Differentiation

Two NPA patient fibroblast lines were reprogrammed to iPSCs, and two iPSC colonies were established for each patient line as HT138C, HT138F from GM13205, and HT139B and HT139E from GM16195 (Fig. 1A; supplemental online Table 1). Cytometric analysis showed that 99% of these iPSCs expressed the pluripotency markers Nanog and the stem cell-specific surface marker Tra-1-60 (Fig. 1C). Further characterization of the patient iPSCs showed a normal karyotype (Fig. 1B). The NPA iPSCs were then differentiated into NSCs with the neural induction medium. The immunofluorescence staining showed that four neural stem cell lines expressed NSC markers, including Nestin, Sox1, and Sox2, and did not display any morphological differences compared with a control line (Fig. 1D). The results demonstrate that four NPA iPSC lines from 2 NPA patients and their differentiated NSCs were successfully established.

NPA Neural Stem Cells Exhibited Sphingomyelin Accumulation and Enlarged Lysosomes

The hallmark of NPA disease is accumulation of SM in lysosomes of patient cells [1, 2]. We used BODIPY-SM to visualize the accumulated sphingomyelin in NPA cells. We found that BODIY-SM was accumulated in lysosomes of NPA NSCs, similar what was observed in the paired NPA fibroblasts (Fig. 2A, 2B). NPA fibroblasts (GM13205 and GM16195) exhibited 2.3- to 2.5-fold increases in lysosomal accumulation of BODIPY-SM compared with that in wild-type (WT) fibroblasts. In NSCs, the BODIY-SM staining increased 2.7-fold in the NPA NSC HT138C line and 1.9- to 2.0-fold in the other three NPA NSC lines compared with that in WT NSCs.

We also examined the enlarged lysosomes in NPA cells due to the accumulation of sphingomyelin by using LysoTracker dye

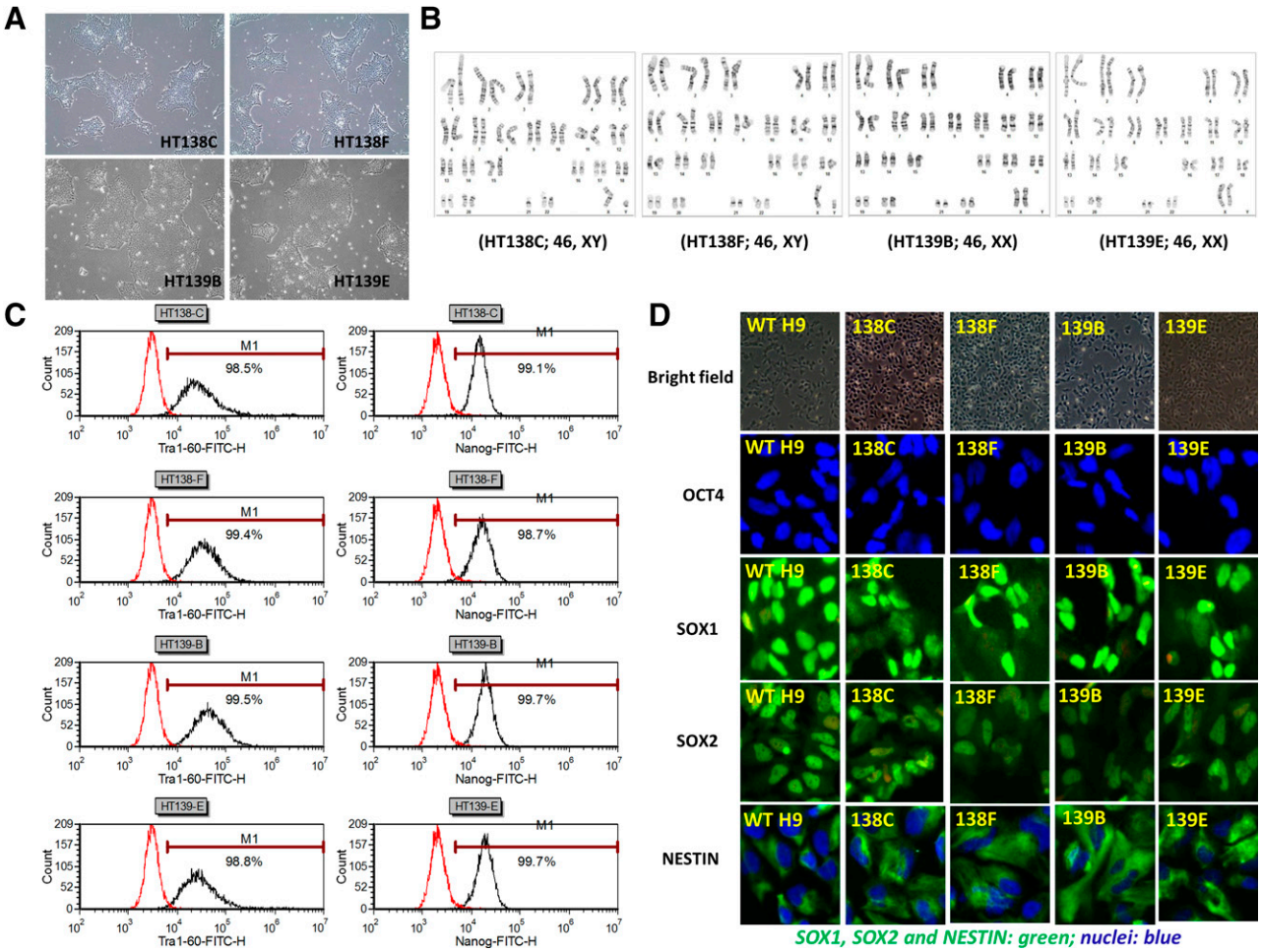

Figure 1. Generation of Niemann-Pick disease type A (NPA)-induced pluripotent stem cells (iPSCs) and neural stem cells (NSCs). **(A):** Images of NPA iPSC colonies from four iPSC lines. **(B):** iPSCs (four lines) derived from two NPA patient fibroblasts displayed normal 46XX or 46XY karyotype. **(C):** Stem cell markers analyzed by flow cytometry. Ninety-nine percent of cells expressed the pluripotency marker Nanog and the stem cell-specific surface marker Tra-1-60. **(D):** Immunofluorescence staining of neural stem cell markers. The four lines of NSCs differentiated from NPA iPSCs exhibited a typical profile of neural stem cell markers. These NSCs showed no morphological differences compared with a control NSC line. The images were taken with a ×20 objective lens. Abbreviations: FITC, fluorescein isothiocyanate; WT, wild type.

staining, which stains cellular acidic compartments. We found elevated LysoTracker staining in both paired NPA fibroblasts and NSCs. LysoTracker dye staining increased 2.7- to 2.9-fold in the NPA GM13205 and GM16195 fibroblast lines compared with that in the WT fibroblasts. In addition, LysoTracker staining increased 1.8- to 2.4-fold in four NPA NSC lines compared with that in control NSCs (Fig. 2C, 2D).

Together, the results revealed significant increase of lysosomal sphingomyelin accumulation and enlargement of lysosomes in all four NPA NSCs differentiated from related iPSCs, similar to those in paired fibroblast lines. The NPA NSCs have the NPA disease phenotype and should serve as a cell-based disease model to study disease pathogenesis and to evaluate drug efficacy.

δ-Tocopherol and α-Tocopherol Reduced Sphingomyelin Accumulation and Enlarged Lysosomal Size in NPA Neural Stem Cells

δ-Tocopherol and α-tocopherol significantly reduced the lysosomal cholesterol accumulation in NPC cells, as well as reduction of enlarged lysosomes in NPA fibroblasts [20]. We examined their effect on reduction of sphingomyelin accumulation and enlarged lysosomes in NPA NSCs. We found that δ-tocopherol concentration dependently reduced sphingomyelin accumulation in the NPA NSCs, similar to those in the paired fibroblasts (Fig. 3A–3C; supplemental online Fig. 1). The half maximal effective concentration (EC_{50}) values were 15.5 μM in the NPA NSC HT138C line and 16.3 μM in the NPA NSC HT138F line, compared with 19.7 μM in the parental GM16195 NPA fibroblast line. Similarly, EC_{50} values were 13.0 μM in the NPA NSC HT139B line and 6.8 μM in the NPA NSC HT139E line, compared with 9.0 μM in the parental GM13205 fibroblast line. The maximum clearance of sphingomyelin accumulation ranged from 33% in the NPA NSC HT138F line to 46% in the NPA NSC HT139E line after treatment with 40 μM δ-tocopherol. In addition, we examined the effect of δ-tocopherol on reduction of LysoTracker red dye staining in NPA NSCs (Fig. 3D–3F). Treatment with 40 μM δ-tocopherol dramatically reduced LysoTracker dye staining in NPA NSCs as well as in the paired fibroblasts (Fig. 3G). Together, the results indicated that δ-tocopherol significantly reduced sphingomyelin accumulation and enlarged lysosomes in the NPA NSCs as well as in the paired NPA fibroblasts.

We also examined the effect of α-tocopherol on reduction of sphingomyelin accumulation and enlarged lysosomes in NPA NSCs. We found that α-tocopherol reduced the sphingomyelin

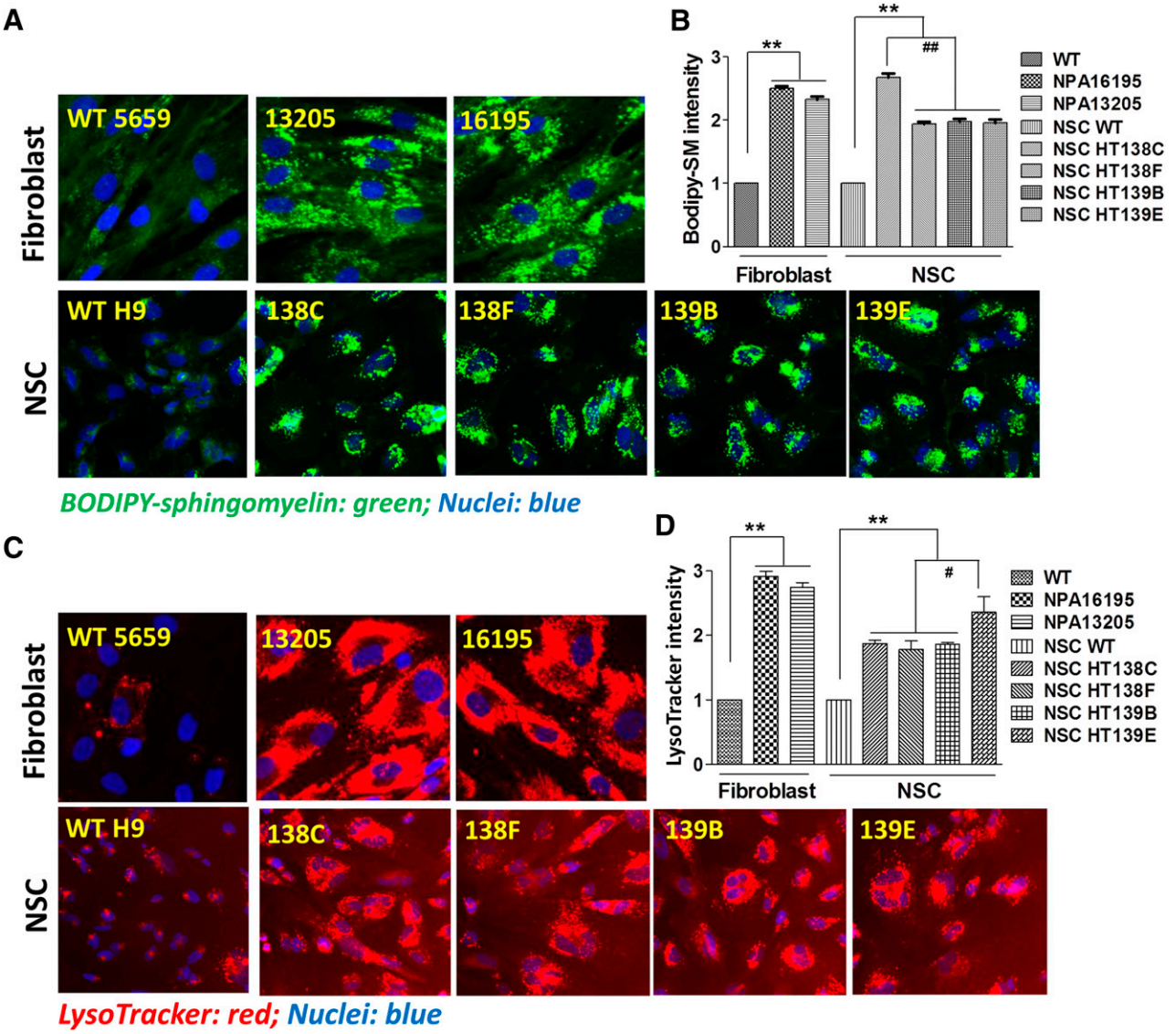

Figure 2. Sphingomyelin accumulation and enlarged lysosomes in Niemann-Pick disease type A (NPA) fibroblasts and NSCs. Sphingomyelin accumulation and enlarged lysosomes are hallmarks of NPA disease. Strong BODIPY-FL C12-sphingomyelin (BODIPY-SM) staining indicates sphingomyelin accumulation **(A),** and increased LysoTracker dye staining **(C)** indicates an enlarged lysosome. Sphingomyelin accumulation and enlarged lysosomes were observed in both parental NPA patient fibroblasts (GM13205 and GM16195) and resulting four NSC lines (HT138C, HT138F, HT139B, and HT139E) compared with the WT fibroblasts (GM5659) and WT NSCs. Quantification of the amount of sphingomyelin **(B)** and acidic compartment **(D)** in fibroblasts and NSCs revealed significantly elevated sphingomyelin levels and enlarged lysosomes in NPA cell lines. The images were taken with a ×20 objective lens. Data are the mean ± SEM. **, $p < .01$ by unpaired Student's *t* test in comparison with WT control cells; #, $p < .05$ in comparison with TH139E NSCs; ##, $p < .01$ in comparison with TH138C NSCs by one-way analysis of variance(Dunnett test). Abbreviations: NSC, neural stem cell; WT, wild type.

accumulation in a concentration-dependent manner in both NSCs and paired fibroblasts (Fig. 4A–4C; supplemental online Fig. 2). The EC_{50} values were 19.7 μM in the NPA NSC HT138F line and 32.2 μM in the NPA NSC HT138C line, compared with 40.9 μM in the parental GM16195 fibroblast line. Similarly, the EC_{50} values were 28.3 μM in the NPA NSC HT139E line and 36.7 μM in the NPA NSC HT139B line, compared with 27.2 μM in the parental GM13205 fibroblast line (Fig. 4A–4C). The maximum inhibition of sphingomyelin accumulation by 80 μM α-tocopherol was 38%–55% in the NPA NSC lines, compared with approximately 17% in both NPA fibroblast lines. A parallel decrease of enlarged lysosomes was also observed as the LysoTracker staining was significantly reduced in NPA NSC lines (Fig. 4D–4F), ranging from 27% to 41% reduction. In contrast to the reduction of LysoTracker staining in NPA NSCs, 20 μM α-tocopherol increased LysoTracker staining by 39%–43% in the NPA GM16195 and GM13205 fibroblast lines compared with the untreated cells (Fig. 4G). Together, the results indicated that α-tocopherol showed a more significant effect on reduction of sphingomyelin accumulation in NPA NSCs, although a higher concentration was needed than with δ-tocopherol.

Hydroxypropyl-β-Cyclodextrin Ameliorated Sphingomyelin Accumulation in NPA Neural Stem Cells

Hydroxypropyl-β-cyclodextrin (HPBCD) was reported to decrease cholesterol accumulation in Niemann Pick disease type C1 (NPC1)

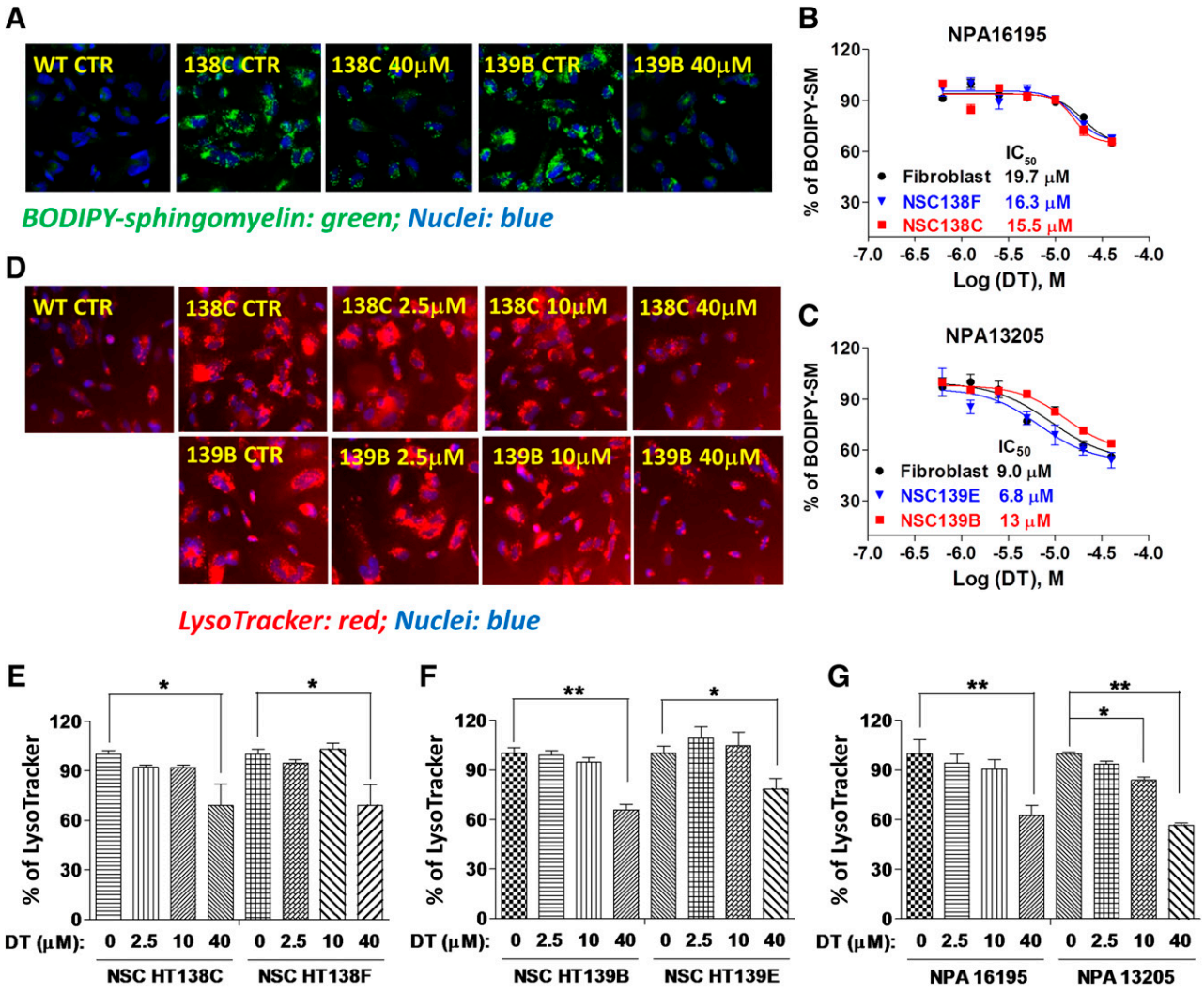

Figure 3. Effect of DT on reducing SM accumulation and enlarged lysosomes in NPA NSCs and fibroblasts. DT concentration dependently reduced the BODIPY-SM staining **(A)** and LysoTracker staining **(D)** in both NPA NSCs and fibroblasts. The half maximal effective concentration (EC_{50}) values of DT on reduction SM accumulation were 15.5 μM in HT138C NSCs, 16.3 μM in HT138F NSCs, and 19.7 μM in the parental NPA GM16195 fibroblasts, respectively **(B)**. The EC_{50} values of DT were 13.0 μM in HT139B NSCs, 6.8 μM in HT139E NSCs, and 9.0 μM in the parental NPA GM13205 fibroblasts, respectively **(C)**. The quantitative analysis of LysoTrackerfluorescence revealed that maximum clearance of enlarged lysosomes ranged from 21% in NSC HT139E **(E, F)** to 43% in NPA GM13205 fibroblasts (**G**) after 40 μM DT treatment. The images were taken with a $\times$20 objective lens. Data are the mean $\pm$ SEM. $*$, $p < .05$ and $**$, $p < .01$ compared with untreated NPA cells analyzed by the unpaired Student's *t* test. Abbreviations: CTR, control; DT, δ-tocopherol; IC_{50}, half maximal inhibitory concentration; M, molar; NPA, Niemann-Pick disease type A; NSC, neural stem cell; SM, sphingomyelin; WT, wild type.

fibroblasts and NSCs [20]. It has also been used as an experimental drug to treat NPC patients [24]. We examined the effect of HPBCD on reduction of sphingomyelin accumulation in NPA NSCs. We found that HPBCD concentration dependently decreased sphingomyelin accumulation in NPA NSCs with EC_{50} values of 1.9, 0.3, 1.6, and 1.0 mM in the NPA NSC HT139B, HT139E, HT138C, and HT138F lines, respectively. The maximum inhibition ranged from 30% to 54% in these NPA NSC lines (Fig. 5A–5C; supplemental online Fig. 3). HPBCD also reduced LysoTracker dye staining in NPA NSCs, with a maximum effect ranging from 25% to 52% in the NPA NSC lines (Fig. 5E, 5F). However, we found that HPBCD increased BODIPY-SM accumulation in NPA fibroblast cell lines by 47%–124% compared with the untreated NPA fibroblasts (Fig. 5G). The results indicated that HPBCD reduced sphingomyelin accumulation and enlarged lysosomes in the NPA NSCs but that its effect in the NPA fibroblasts was different.

We also tried to determine the synergistic effect of HPBCD with δ-tocopherol on reduction of sphingomyelin accumulation in NPA NSCs. The treatment of NPA NSCs with a combination of HPBCD and δ-tocopherol did not further improve the effect of δ-tocopherol on sphingomyelin accumulation in these cells (supplemental online Figs. 4, 5; Table 1).

ASM Treatment Reduced Sphingomyelin Accumulation in NPA NSCs

We also evaluated the effect of exogenous ASM in the NPA NSCs as the ERT. The exogenous ASM was incubated with the NPA NSCs for

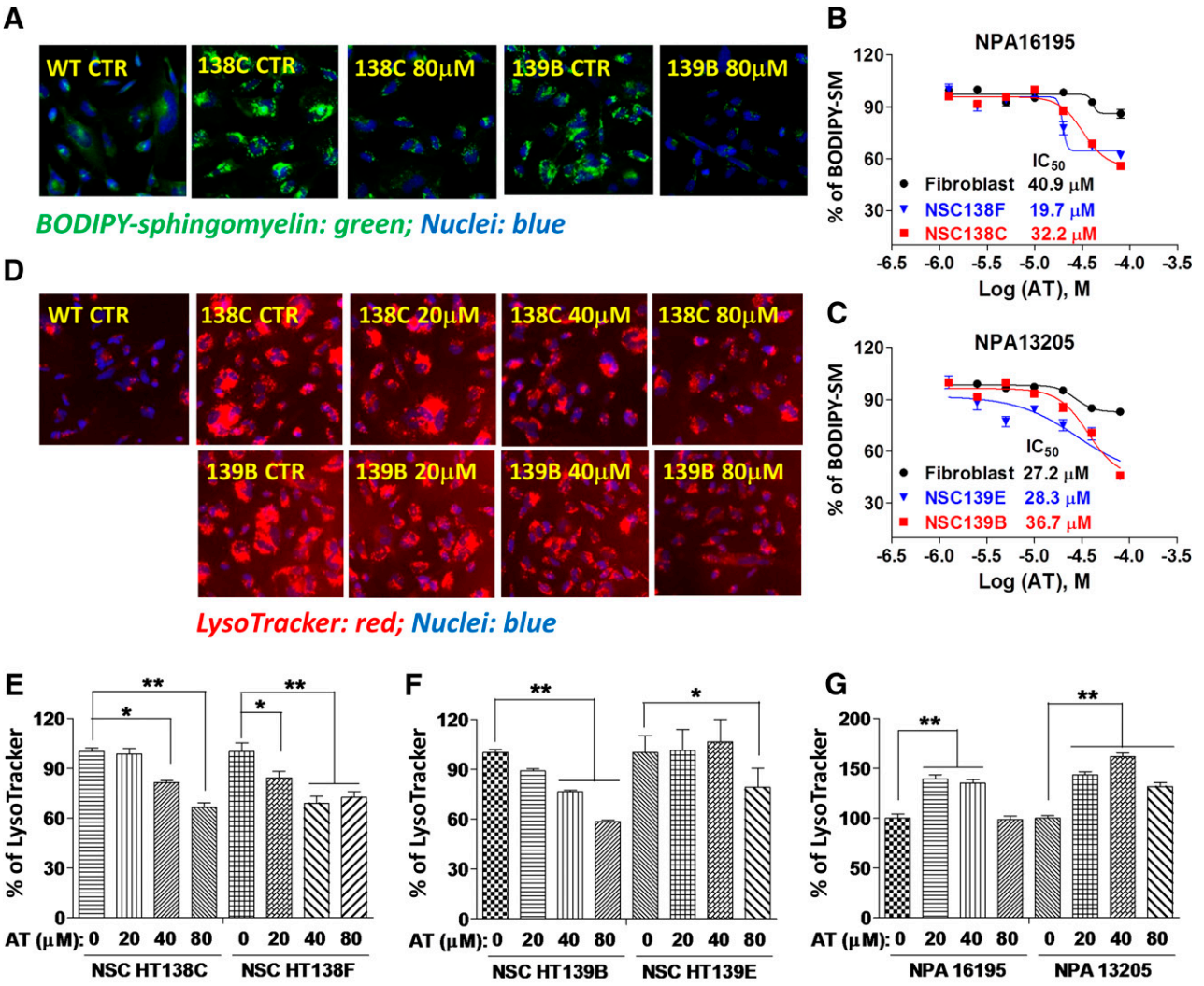

Figure 4. AT decreased SM accumulation and enlarged lysosomes in NPA NSCs and fibroblasts. **(A):** BODIPY-SM staining. Fluorescent microscopic images of NPA NSCs and fibroblasts treated with 80 μM AT for 3 days. **(B, C):** Concentration responses of AT on reduction of BODIPY-SM staining in NPA cells. The half maximal effective concentration (EC_{50}) values of AT were 19.7 μM in HT138F NSCs, 32.2 μM in HT138C NSCs, and 40.9 μM in the parental GM16195 fibroblasts, respectively. The EC_{50} values of AT were 28.3 μM in HT139E NSCs, 36.7 μM in HT139B NSCs, and 27.2 μM in the parental GM13205 fibroblasts, respectively. **(D):** Images of LysoTracker staining in NPA cells after the treatment with AT for 4 days. **(E, F):** The maximum reduction of enlarged lysosomes ranged from 27% in HT138F NSCs to 41% in NSC HT139B after 80 μM AT treatment. **(G):** In contrast, 20 μM AT caused 39% and 43% increases in LysoTracker staining in the NPA GM16195 and GM13205 fibroblasts compared with untreated cells. The images were taken with a $\times$20 objective lens. Data are the mean $\pm$ SEM. $*$, $p < .05$ and $**$, $p < .01$ compared with untreated NPA cells analyzed by the unpaired Student's *t* test. Abbreviations: AT, α-tocopherol; IC_{50}, half maximal inhibitory concentration; NPA, Niemann-Pick disease type A; NSC, neural stem cell; SM, sphingomyelin; WT, wild type.

4 hours before BODIPY-SM was loaded to these cells, followed by 24-hour incubation. The treatment of NPA NSCs with 187.5 nM ASM reduced sphingomyelin accumulation in the NPA HT138C and HT139B NSC lines (Fig. 6A, 6B). The results indicated that the sphingomyelin in lysosomes could be hydrolyzed by the exogenous acid sphingomyelinase, which entered cells through the endocytic pathway.

Correction of Ultrastructural Pathology by α-Tocopherol, δ-Tocopherol, and HPBCD in NPA NSCs

To examine whether α-tocopherol, δ-tocopherol, and HPBCD improve ultrastructural features in the NPA NSCs, we carried out electron microscopy analysis in the NPA HT138C NSCs (Fig. 6C–6H). The abundant lysosomal multilamellar and multivesicular bodies near the nucleus were observed in NPA HT138C NSCs (Fig. 6D) that were not present in WT cells (Fig. 6C). These lamellar bodies were compact and were frequently found within the boundaries of a vacuole (Fig. 6D). After treatment with 30 $\mu\delta$-tocopherol, 30 μM δ-tocopherol plus 30 μHPBCD, 60 μM α-tocopherol, or 3 mM HPBCD for 3 days, the lysosomal multilamellar and multivesicular bodies were dramatically reduced (Fig. 6E–6H). In addition, the lamellar bodies were much less compact and less frequent in number. These lysosomal multilamellar bodies were often found near the plasma membrane, and in a few examples there were ruptures at the site of plasma membrane where there was lysosomal content (multilamellar multivesicular bodies), suggesting

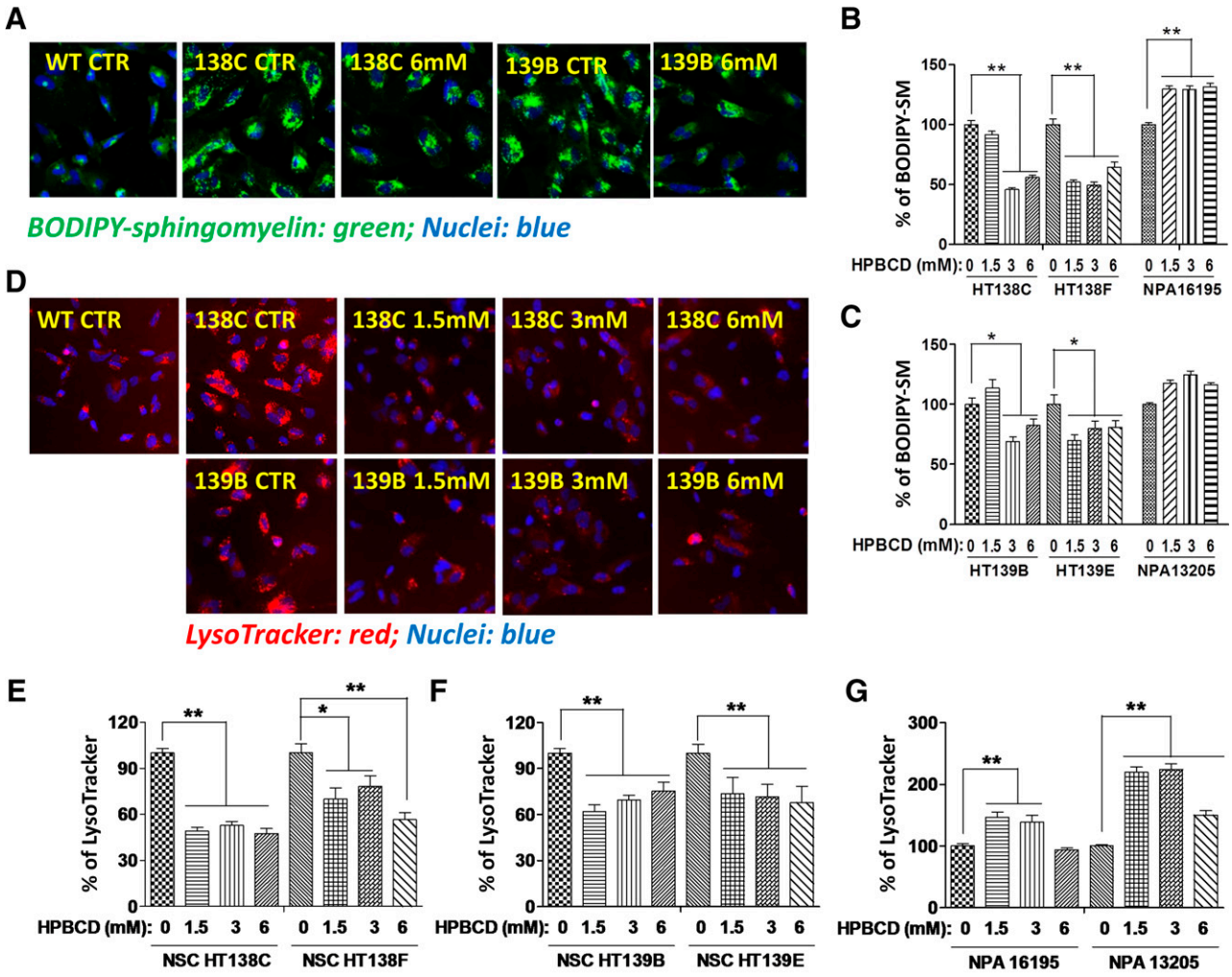

Figure 5. HPBCD ameliorated the SM accumulation and enlarged lysosomes in NPA NSCs. **(A–C):** Fluorescent images and quantitative analysis of HPBCD's effect on reduction of BODIPY-SM staining in NPA NSCs and fibroblasts. The half maximal effective concentration values of HPBCD were 1.9 mM in HT139B NSCs, 0.3 mM in HT139E NSCs, 1.6 mM in HT138C NSCs, and 1.0 mM in HT138F NSCs, respectively. However, 1.5 mM HPBCD increased the BODIPY-SM staining by 25% in the NPA GM16195 fibroblasts. **(D–G):** Images and quantitative analysis of LysoTracker staining in NPA NSCs and fibroblasts. The maximum reduction of enlarged lysosomes ranged from 25% in HT139B NSCs to 52% in HT138C NSCs after 6 mM HPBCD treatment **(E, F)**. In contrast, 1.5 mM HPBCD caused 47% and 124% increases of LysoTracker staining in the NPA GM16195 and GM13205 fibroblast lines compared with the untreated NPA cells **(G)**. The images were taken with a $\times 20$ objective lens. Data are the mean $\pm$ SEM. $*$, $p < .05$ and $**$, $p < .01$ compared with the untreated NPA cells analyzed by the unpaired Student's t test. Abbreviations: HPBCD, hydroxypropyl-β-cyclodextrin; NPA, Niemann-Pick disease type A; NSC, neural stem cell; SM, sphingomyelin; WT, wild type.

that they would be released to the extracellular space. Among the treatments described here, 60 μM α-tocopherol (Fig. 6H) and 30 μM δ-tocopherol plus 30 μM HPBCD (Fig. 6F) produced the most significant effect. The ultrastructural morphology of the NPA NSCs after treatments with α-tocopherol and 30 μM δ-tocopherol plus 30 μM HPBCD appeared almost like normal cells. The number of small vacuoles was dramatically decreased, with almost clean or less cellular debris. The multilamellar bodies were drastically reduced in size, intensity, and number.

In summary, we generated four NPA iPSC lines from two NPA patient fibroblast lines. Four NPA NSC lines were also differentiated from these iPSC lines. These NPA NSCs exhibited the characteristic NPA phenotype of sphingomyelin accumulation and enlarged lysosomes that can serve as a cell-based disease model for study of disease pathophysiology and for evaluation of compound therapeutic efficacy. We also found that δ-tocopherol exhibited similar activities on reduction of sphingomyelin accumulation and enlarged lysosomes in both NPA NSCs and their parental fibroblasts, whereas α-tocopherol and HPBCD showed their activity only in the NPA NSCs. In addition, α-tocopherol and the combination of δ-tocopherol plus HPBCD almost completely ameliorated sphingomyelin accumulation in NPA NSCs at higher concentrations, specially evidenced by the electron microscopic analysis. HPBCD's effect on reduction of lysosomal sphingomyelin accumulation was weaker than the effect of tocopherols in human NPA NSCs. ERT with purified acid sphingomyelinase also reduced the disease phenotype in the NPA NSCs. The results also revealed a significant difference in drug responses to α-tocopherol and HPBCD between NPA neuronal cells and fibroblasts, although they were derived from the same NPA patients, whereas δ-tocopherol exhibited similar effects in both NPA NSCs and parental fibroblasts.

Table 1. Half maximal effective concentration values of δ-tocopherol, α-tocopherol, and hydroxypropyl-β-cyclodextrin on Neumann-Pick disease type A fibroblasts and neural stem cells

	EC_{50}									
	DT (μM)		AT (μM)		HPBCD (mM)		DT+30 μM HPBCD (μM)		DT+100 μM HPBCD (μM)	
Variable	BODIPY	Lyso	BODIPY	Lyso	BODIPY	Lyso	BODIPY	Lyso	BODIPY	Lyso
GM 16195	19.7	19.3	40.9	1.7 (+)	0.3 (+)	0.2 (+)	8.4	36.5	18.3	17.1
GM 13205	9.0	12.5	27.2	2.9 (+)	0.2 (+)	0.3 (+)	9.8	26.4	16.7	16.3
NSC HT138C	15.5	17.8	32.2	36.1	1.6	0.2	16.0	10.5	9.4	3.4
NSC HT138F	16.3	16.5	19.7	19.7	1.0	0.4	16.2	21.9	11.6	5.2
NSC HT139B	13.0	27.2	36.7	33.0	1.9	0.2	2.5	42.8	9.5	9.6
NSC HT139E	6.8	34.0	28.3	55.7	0.3	0.3	10.3	39.3	1.9	9.7

Abbreviations: +, increase of staining; AT, α-tocopherol; DT, δ-tocopherol; EC_{50}, half maximal effective concentration; HPBCD, hydroxypropyl-β-cyclodextrin; Lyso, LysoTracker red staining; NSC, neural stem cell.

Discussion

NPA causes neuronal degeneration and exhibits major clinical presentations in the central nervous system. Therefore, patient-derived neuronal cells are a proper model system for study of disease pathogenesis and evaluation of compound efficacy for drug development. We have successfully generated four iPSC lines from two NPA patient dermal fibroblast cell lines using the nonintegrating CytoTune-Sendai virus reprogramming method. These iPSCs have also been differentiated into NSCs, which exhibited the characteristic NPA disease phenotype of sphingomyelin accumulation and enlarged lysosomes. This cell-based NPA model was used to evaluate the effects of α-tocopherol, δ-tocopherol, and HPBCD on amelioration of NPA disease phenotype. These three compounds showed positive effects on the NPA NSCs, although HPBCD showed an opposite effect on the paired NPA fibroblasts. Our results demonstrate that the NPA NSCs are a better disease model than NPA fibroblasts. These patient-derived NSCs can be used as a cell-based NPA disease model for further study of disease pathophysiology and screening of compound libraries for drug development.

Application of patient iPSCs for modeling disease phenotype has emerged as a new approach for drug discovery and development [25, 26]. Many neurological diseases do not have disease-relevant animal models, which has greatly limited the ability for evaluation of drug efficacy for drug development. The recent available methods of differentiation of patient iPSCs to nature cells, such as neuronal cells, cardiomyocytes, and hepatocytes, also provide new cell-based disease models for phenotypic drug screens [27]. To date, six human iPSC lines have been reported for 50 lysosomal storage diseases, including Gaucher disease [28, 29], MPS I [30], MPS IIIB [31], Pompe disease [32], Fabry disease [33], and NPC1 [20]. The generation of NPA iPSCs contributes to the collections of new cell-based disease models for lysosomal storage diseases. These four NPA iPSC lines represent two different *SMPD1* gene mutations, including a T-C transition in the nucleotide 905 (L302P) and a deletion of a cytosine in codon 330 (fsP330) (supplemental online Table 1) [34]. Both are common mutations in the Ashkenazi Jewish population, although there are no common mutations in the *SMPD1* gene in the general population [4]. Both NPA iPSCs and neural stem cells differentiated from these iPSCs displayed normal morphologies and multiple markers (Fig. 1). No obvious abnormality was observed for NPA iPSCs and differentiated NPA NSCs. These four NPA iPSC lines had been cultured for 15 passages without significant changes in their morphology and growth rate.

The differentiated NPA NSCs exhibited characteristic disease phenotype of lysosomal sphingomyelin accumulation and enlargement of lysosomal sizes (Fig. 2), similar to the paired NPA patient-derived fibroblasts. Neural stem cells are self-renewable and can be produced in large quantity for compound screening. Compared with differentiated neurons, NSCs are more readily adapted into the high-throughput screening for lead discovery and drug efficacy evaluation. Several laboratories had reported to use iPSC differentiated neural stem cells and neural progenitor cells for high-throughput compound screening to identify lead compounds for drug development [25, 35]. Because the NPA NSCs have the NPA disease phenotype and can be produced in large quantity, they should serve as a disease-relevant model system for drug screening.

α-Tocopherol and δ-tocopherol belong to the eight components of vitamin E that reportedly reduce lysosomal cholesterol accumulation in patient cells derived from NPC [19, 20]. The mechanism of action of the tocopherols was linked to an increase in lysosomal exocytosis in the patient cells [19]. Therefore, we examined the potential therapeutic effect of these tocopherols in the NPA NSCs. Our results showed that both tocopherols exhibited dose-dependent inhibition of the sphingomyelin accumulation in NPA NSCs (Figs. 3, 4; supplemental online Figs. 1, 2).

HPBCD is a complex cyclic carbohydrate composed of seven glycosidic residues assembled into a ring structure [36, 37]. It has been approved for use as an excipient in the drug formulation for delivery of lipid soluble compounds, in which it forms an inclusion complex with a hydrophobic small molecule through its hydrophobic cavity formed by the sugar ring [37]. The effect of HPBCD on reduction of lysosomal cholesterol accumulation was observed in the NPC patient cells [20] and animal models [38–40]. Recently, HPBCD has been used in clinical trials to treat NPC patients [24]. In the present study, the results showed that HPBCD concentration dependently alleviated the lysosomal sphingomyelin accumulation and enlarged lysosomes in differentiated NPA neural stem cells but not in the original NPA fibroblasts (Fig. 5; supplemental online Fig. 3). The result also suggested different responses of HPBCD in different cell types from the same NPA patient. Because the main pathological changes of NPA occur in the central nervous system, neuronal cells are obviously more representative as a disease model system than the patient fibroblasts.

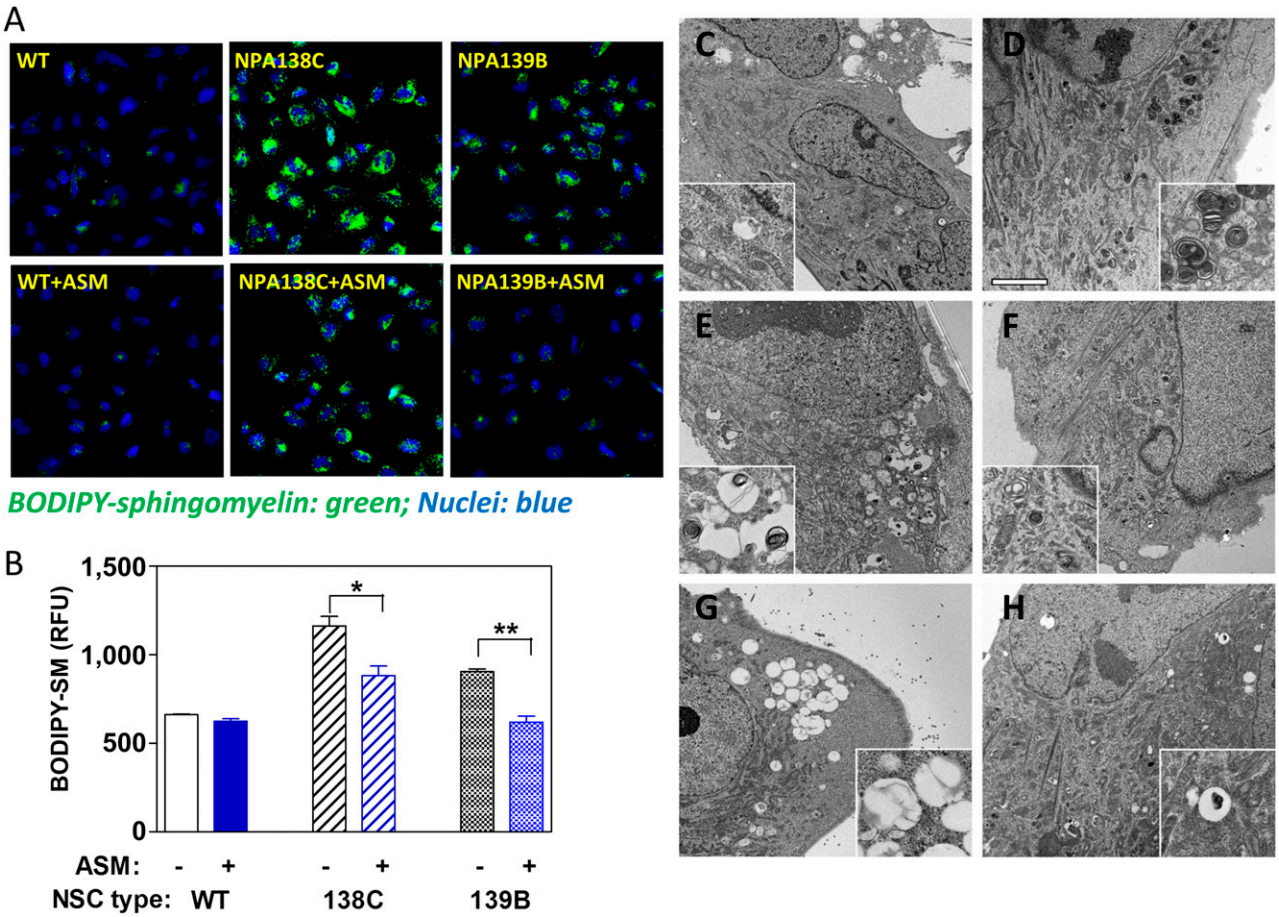

Figure 6. Reduction of sphingomyelin accumulation by ASM and amelioration of ultrastructural pathology by α-tocopherol, δ-tocopherol, and hydroxypropyl-β-cyclodextrin (HPBCD) in NPA neural stem cell (NSCs). **(A):** Fluorescent images of BODIPY-SM staining in NPA NSCs after treatment with ASM in NPA 138C and 139B NSC lines in comparison with an induced pluripotent stem cell-derived WT NSC line. The NPA NSCs were treated with 187.5 nM ASM for 4 hours before the 24-hour incubation with BODIPY-SM. **(B):** Quantitative analysis of reduction of sphingomyelin accumulation in NPA NSCs by ASM treatment. Data are the mean $\pm$ SEM. $*$, $p < .05$ and $**$, $p < .01$ compared with the untreated NPA cells analyzed by the unpaired Student's *t* test. The images were taken with a $\times 20$ objective lens. Electron micrographs of thin sections of NSC of **(C)** healthy control, **(D)** untreated NPA, and NPA cells treated with **(E)** 30 μM δ-tocopherol, **(F)** 30 μM δ-tocopherol and 30 μM HPBCD, **(G)** 3 mM HPBCD, and **(H)** 60 μM α-tocopherol. The inset shows higher-magnification examples of the typical multilamellar and multivesicular bodies in cases in which they are present. In **(C)**, **(F)**, and **(H),** none of these structures are present. The scale bar represents 5 μm in the main panels and 1.5 μm in the insets. Abbreviations: ASM, acid sphingomyelinase; NPA, Niemann-Pick disease type A; RFU, relative fluorescence unit; SM, sphingomyelin; WT, wild type.

Treatment of NPA NSCs with tocopherols and cyclodextrin also corrected the ultrastructural pathology in NPA neuronal cells (Fig. 6E–6H). α-Tocopherol showed the most notable clearance potency of intracellular sphingomyelin accumulation in NPA NSCs with the disappearance of multilamellar or multivesicular bodies in the lysosomes. The mechanism of tocopherols on reduction of sphingomyelin accumulation could be similar to the upregulated lysosomal exocytosis [19]. The microscopic analysis also showed a synergistic/additive effect of a combination of tocopherol and cyclodextrin in NPA NSCs, although the effect was not significant in the fluorescence dye staining experiments (BODIPY-SM and LysoTracker dye staining).

In the present study, the results reported were based only on the iPSC lines generated from two NPA patient samples. Additional research with more NPA patient samples is needed to determine a correlation of disease phenotype in NSCs with clinical symptoms, although such an effort requires a huge amount of resources. In addition, three obstacles hinder the large scale of drug screening using the NPA NSCs. First, the assay plates have to be precoated with extracellular matrix proteins (CELLstart) involving multiple steps of reagent/buffer addition and plate wash. This process not only reduces screening throughput but also yields large well-to-well and plate-to-plate variations. This precoating of plates is bottleneck for using neuronal cells in high throughput screening [41]. Second, frequent medium changes are required for culture neural stem cells in assay plates because of the extreme vulnerability of these cells; such medium changes are not practical in 384- and 1,536-well plates for high-throughput screening. Third, the reagents for culturing neural stem cells have high cost, which also limits the use of iPSC differentiated neural stem cells and neurons for high-throughput screening. New methods and new approaches are needed for future application of iPSC differentiated neural stem cells and neurons for high-throughput screening.

Conclusion

We have generated NPA iPSCs from two patient samples and established two cell-based assays (BODIPY-SM and LysoTracker dye staining) using the differentiated neural stem cells to model NPA disease phenotype. We have used this NPA disease model to evaluate drug efficacy of three drugs as well as ERT. The effects of α-tocopherol, δ-tocopherol, HPBCD, and acid sphingomyelinase on reduction of lysosomal sphingomyelin accumulation were confirmed in this cell-based NPA disease model. Therefore, this model can be used for further study of disease pathophysiology and for evaluation of drug efficacy.

Acknowledgments

This work was supported by the Intramural Research Programs of the National Center for Advancing Translational Sciences. This work was also supported by grants from the China Scholarship Council and grants from the National Natural Science Foundation of China (81503170 to Y.L.) and Guangdong Natural Science Foundation (2016A030313170 to Y.L.), from federal funds from the Frederick National Laboratory for Cancer Research, National Institutes of Health (under contract HHSN26120080001E to U.B. and F.S.), from the Natural Science Foundation of Zhejiang Province for Distinguished Young Scholars (LR14H090001 to M. X.), from the National Institutes of Health (R01-HL098416 to S. M.), and from the University of Macau (MYRG2015-00228-FHS to G.C.).

Author Contributions

Y.L., conception and design, data acquisition, analysis, and interpretation, manuscript writing; M.X., R.L., S.D., and M.W.: data acquisition, analysis, and interpretation; J.J.M., S.M., Z.L., and R.B.: conception and design, data interpretation, manuscript writing; J.B. and G.C.: iPSC generation; F.S. and U.B.: electron microscopic analysis; W.Z.: conception and design, data interpretation, manuscript writing, provision of support, final approval of manuscript.

Disclosure of Potential Conflicts of Interest

The authors indicated no potential conflicts of interest.

References

1 Schuchman EH. The pathogenesis and treatment of acid sphingomyelinase-deficient Niemann-Pick disease. J Inherit Metab Dis 2007;30:654–663.

2 Brady RO, Kanfer JN, Mock MB et al. The metabolism of sphingomyelin. II. Evidence of an enzymatic deficiency in Niemann-Pick diseae. Proc Natl Acad Sci USA 1966;55: 366–369.

3 Ledesma MD, Prinetti A, Sonnino S et al. Brain pathology in Niemann Pick disease type A: insights from the acid sphingomyelinase knockout mice. J Neurochem 2011;116:779–788.

4 Schuchman EH, Miranda SR. Niemann-Pick disease: Mutation update, genotype/phenotype correlations, and prospects for genetic testing. Genet Test 1997;1:13–19.

5 Futerman AH, van Meer G. The cell biology of lysosomal storage disorders. Nat Rev Mol Cell Biol 2004;5:554–565.

6 Zhang H, Wang Y, Gong Z et al. Identification of a distinct mutation spectrum in the SMPD1 gene of Chinese patients with acid sphingomyelinase-deficient Niemann-Pick disease. Orphanet J Rare Dis 2013;8:15.

7 Hollak CE, de Sonnaville ES, Cassiman D et al. Acid sphingomyelinase (ASM) deficiency patients in The Netherlands and Belgium: Disease spectrum and natural course in attenuated patients. Mol Genet Metab 2012;107:526–533.

8 Schuchman EH. The pathogenesis and treatment of acid sphingomyelinase-deficient Niemann-Pick disease. Int J Clin Pharmacol Ther 2009;47(Suppl 1):S48–S57.

9 Beck M. New therapeutic options for lysosomal storage disorders: Enzyme replacement, small molecules and gene therapy. Hum Genet 2007;121:1–22.

10 Desnick RJ, Schuchman EH. Enzyme replacement and enhancement therapies: Lessons from lysosomal disorders. Nat Rev Genet 2002;3:954–966.

11 Bu J, Ashe KM, Bringas J et al. Merits of combination cortical, subcortical, and cerebellar injections for the treatment of Niemann-Pick disease type A. Mol Ther 2012;20:1893–1901.

12 Gray SJ, Matagne V, Bachaboina L et al. Preclinical differences of intravascular AAV9 delivery to neurons and glia: A comparative study of adult mice and nonhuman primates. Mol Ther 2011;19:1058–1069.

13 Bu J, Ashe KM, Bringas J et al. Merits of combination cortical, subcortical, and cerebellar injections for the treatment of Niemann-Pick disease type A. Mol Ther 2012;20:1893–1901.

14 Gray SJ, Matagne V, Bachaboina L et al. Preclinical differences of intravascular AAV9 delivery to neurons and glia: A comparative study of adult mice and nonhuman primates. Mol Ther 2011;19:1058–1069.

15 Papademetriou J, Garnacho C, Serrano D et al. Comparative binding, endocytosis, and biodistribution of antibodies and antibody-coated carriers for targeted delivery of lysosomal enzymes to ICAM-1 versus transferrin receptor. J Inherit Metab Dis 2013;36: 467–477.

16 Malatack JJ, Consolini DM, Bayever E. The status of hematopoietic stem cell transplantation in lysosomal storage disease. Pediatr Neurol 2003;29:391–403.

17 Ficicioglu C. Review of miglustat for clinical management in Gaucher disease type 1. Ther Clin Risk Manag 2008;4:425–431.

18 Valenzano KJ, Khanna R, Powe AC et al. Identification and characterization of pharmacological chaperones to correct enzyme deficiencies in lysosomal storage disorders. Assay Drug Dev Technol 2011;9:213–235.

19 Xu M, Liu K, Swaroop M et al. δ-Tocopherol reduces lipid accumulation in Niemann-Pick type C1 and Wolman cholesterol storage disorders. J Biol Chem 2012;287:39349–39360.

20 Yu D, Swaroop M, Wang M et al. Niemann-Pick disease type C: Induced pluripotent stem cell-derived neuronal cells for modeling neural disease and evaluating drug efficacy. J Biomol Screen 2014;19:1164–1173.

21 Rappaport J, Manthe RL, Solomon M et al. A comparative study on the alterations of endocytic pathways in multiple lysosomal storage disorders. Mol Pharm 2016;13:357–368.

22 Beers J, Gulbranson DR, George N et al. Passaging and colony expansion of human pluripotent stem cells by enzyme-free dissociation in chemically defined culture conditions. Nat Protoc 2012;7:2029–2040.

23 Muro S, Schuchman EH, Muzykantov VR. Lysosomal enzyme delivery by ICAM-1-targeted nanocarriers bypassing glycosylation- and clathrin-dependent endocytosis. Mol Ther 2006;13:135–141.

24 Matsuo M, Togawa M, Hirabaru K et al. Effects of cyclodextrin in two patients with Niemann-Pick Type C disease. Mol Genet Metab 2013;108:76–81.

25 Engle SJ, Puppala D. Integrating human pluripotent stem cells into drug development. Cell Stem Cell 2013;12:669–677.

26 Lee G, Ramirez CN, Kim H et al. Large-scale screening using familial dysautonomia induced pluripotent stem cells identifies compounds that rescue IKBKAP expression. Nat Biotechnol 2012; 30:1244–1248.

27 Rao M. iPSC crowdsourcing: A model for obtaining large panels of stem cell lines for screening. Cell Stem Cell 2013;13:389–391.

28 Tiscornia G, Vivas EL, Matalonga L et al. Neuronopathic Gaucher's disease: Induced pluripotent stem cells for disease modelling and testing chaperone activity of small compounds. Hum Mol Genet 2013; 22:633–645.

29 Panicker LM, Miller D, Park TS et al. Induced pluripotent stem cell model recapitulates pathologic hallmarks of Gaucher disease. Proc Natl Acad Sci USA 2012;109: 18054–18059.

30 Tolar J, Park IH, Xia L et al. Hematopoietic differentiation of induced pluripotent stem cells from patients with mucopolysaccharidosis

type I (Hurler syndrome). Blood 2011;117: 839–847.

31 Lemonnier T, Blanchard S, Toli D et al. Modeling neuronal defects associated with a lysosomal disorder using patient-derived induced pluripotent stem cells. Hum Mol Genet 2011; 20:3653–3666.

32 Huang HP, Chen PH, Hwu WL et al. Human Pompe disease-induced pluripotent stem cells for pathogenesis modeling, drug testing and disease marker identification. Hum Mol Genet 2011;20:4851–4864.

33 Kawagoe S, Higuchi T, Otaka M et al. Morphological features of iPS cells generated from Fabry disease skin fibroblasts using Sendai virus vector (SeVdp). Mol Genet Metab 2013;109: 386–389.

34 Levran O, Desnick RJ, Schuchman EH. Identification and expression of a common missense mutation (L302P) in the acid sphingomyelinase gene of Ashkenazi Jewish type A Niemann-Pick disease patients. Blood 1992; 80:2081–2087.

35 Rowntree RK, McNeish JD. Induced pluripotent stem cells: Opportunities as research and development tools in 21st century drug discovery. Regen Med 2010;5: 557–568.

36 Szejtli J. Introduction and general overview of cyclodextrin chemistry. Chem Rev 1998;98:1743–1754.

37 Vecsernyés M, Fenyvesi F, Bácskay I et al. Cyclodextrins, blood-brain barrier, and treatment of neurological diseases. Arch Med Res 2014;45:711–729.

38 Camargo F, Erickson RP, Garver WS et al. Cyclodextrins in the treatment of a mouse model of Niemann-Pick C disease. Life Sci 2001;70:131–142.

39 Taylor AM, Liu B, Mari Y et al. Cyclodextrin mediates rapid changes in lipid balance in Npc1-/- mice without carrying cholesterol through the bloodstream. J Lipid Res 2012; 53:2331–2342.

40 Tanaka Y, Yamada Y, Ishitsuka Y et al. Efficacy of 2-hydroxypropyl-β-cyclodextrin in Niemann-Pick disease type C model mice and its pharmacokinetic analysis in a patient with the disease. Biol Pharm Bull 2015;38:844–851.

41 Villa-Diaz LG, Ross AM, Lahann J et al. Concise review: The evolution of human pluripotent stem cell culture: From feeder cells to synthetic coatings. STEM CELLS 2013;31:1–7.

See www.StemCellsTM.com for supporting information available online.

